IOP Publishing Superconductor Science and Technology
Supercond. Sci. Technol. 31 (2018) 115005 (7pp) https://doi.org/10.1088/1361-6668/aade5a

Superconductivity in the superhard boride $WB_{4.2}$

Elizabeth M Carnicom[1,6], Judyta Strychalska-Nowak[2], P Wiśniewski[3], D Kaczorowski[3,4], W Xie[5], T Klimczuk[2] and R J Cava[1,6]

[1] Department of Chemistry, Princeton University, Princeton, NJ 08544, United States of America
[2] Department of Physics, Gdansk University of Technology, Gdansk 80-233, Poland
[3] Institute of Low Temperature and Structure Research, Polish Academy of Sciences, PNr 1410, 50-950 Wrocław, Poland
[4] Institute of Molecular Physics, Polish Academy of Sciences, Mariana Smoluchowskiego 17, 60-179 Poznań, Poland
[5] Department of Chemistry, Louisiana State University, Baton Rouge, LA 70803, United States of America

E-mail: carnicom@princeton.edu and rcava@exchange.princeton.edu

Received 24 August 2018
Accepted for publication 3 September 2018
Published 27 September 2018

Abstract

We show that the superhard boride $WB_{4.2}$ is a superconductor with a T_c of 2.05(5) K. Temperature-dependent magnetic susceptibility, electrical resistivity, and specific heat measurements were used to characterize the superconducting transition. The Sommerfeld constant γ for $WB_{4.2}$ is 2.07(3) mJ mol^{-1} K^{-2} and the $\Delta C/\gamma T_c = 1.56$, which is somewhat higher than what is expected for weakly coupled Bardeen–Cooper–Schrieffer type superconductors. The H_{c2} versus T plot is linear over a wide temperature range but does show signs of flattening by the lowest temperatures studied and therefore the zero temperature upper critical field ($\mu_0 H_{c2}(0)$) for $WB_{4.2}$ lies somewhere between the linear extrapolation of $\mu_0 H_{c2}(T)$ to 0 K and expectations based on the Werthamer–Helfand–Hohenberg model.

Keywords: superconductivity, superhard, tungsten deficient, boride

(Some figures may appear in colour only in the online journal)

Introduction

High superconducting transition temperatures may be anticipated for borides due to boron's light mass and strong B–B covalent bonding, which yields high vibrational frequencies. Superconductivity has been discovered in metal diborides like MgB_2 ($T_c = 39$ K [1]), $(Mo_{0.96}Zr_{0.04})_{0.85}B_2$ ($T_c = 8.2$ K [2]), NbB_2 ($T_c = 5.2$ K [3]) and various other ternary borides [4–7]. Often the superconducting early transition metal 'diborides' are deficient in metal content, such as is seen in $Nb_{0.76}B_2$, which is deficient in Nb [8–10]. The metal deficiencies can sometimes be described by the general formula $T_{1-\delta}B_{2+3\delta}$ where every time a transition metal (T) is removed, 3 B atoms are added to the structure. Moreover, in these metal borides, boron atoms are likely to bond strongly with each other and form various molecule-like boron clusters, such as in the honeycomb lattice sheets of boron in MgB_2.

The strong B–B covalent bonding is not only attractive in superconducting materials but also in superhard materials, which have been extensively studied, especially for their practical use as cutting tools, abrasives, or wear-resistant coatings in various industrial applications [11–19]. Diamond and a variety of light-element compounds, although superhard materials, have practical and synthetic limitations for some applications [20–23] motivating the search for other types of superhard materials [24] like metal borides, which are an important class of superhard materials that can be easily synthesized. The well-known superhard metal diborides are RuB_2 [25], OsB_2 [24, 26], and ReB_2 [27, 28]. In addition, superconductivity has been reported in the superhard material FeB_4 [29]. The shared characteristics of metal borides that link superconductors and superhard materials motivated us to study the superconducting properties of superhard materials.

WB_4, the subject of the current work, is also a superhard material, with a hardness of 43 GPa [30]. Structurally, WB_4

[6] Authors to whom any correspondence should be addressed.

has been of particular interest because most other transition metals besides tungsten cannot tolerate higher boron contents and therefore exist as diborides [31, 32]. Most studies since the discovery of WB_4 [33] have found the crystal structure to have hexagonal symmetry, but there are a range of reported formulas such as WB_4 [32], $WB_{4.92}$ [34], $W_{1-x}B_3$ [35], or $WB_{4.2}$ [36]. The lattermost case is most consistent with our work.

Here we report the crystal structure and basic superconducting properties of the superhard boride $WB_{4.2}$. Our single crystal x-ray diffraction characterization shows, in agreement with earlier work, that $WB_{4.2}$ crystallizes in the space group $P6_3/mmc$ (No. 194) and has a crystal structure that is derived from the simple diborides but with a systematic W-deficiency-B_3 substitution—each missing W atom in the 2*b* position is replaced by three B atoms in the 6*h* position. Different experiments show sharp and reproducible superconducting transitions at about 2 K for $WB_{4.2}$. Temperature-dependent magnetic susceptibility, electrical resistivity and specific heat measurements were used to characterize the superconductor. $WB_{4.2}$ is a Bardeen–Cooper–Schrieffer (BCS)-type superconductor with an upper critical magnetic field, $H_{c2}(0)$, that is between that predicted by the standard WHH equation and the result of using a linear extrapolation of $H_{c2}(T)$ to zero temperature.

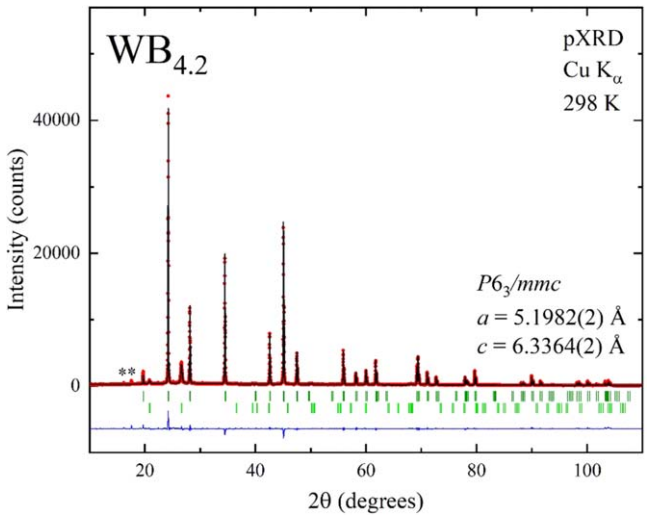

Figure 1. Rietveld refinement of room temperature powder x-ray diffraction data for $WB_{4.2}$. The red circles are the observed data, the black line is the calculated fit, the dark green vertical bars are the expected Bragg reflections for $WB_{4.2}$, and the light green vertical bars are the expected Bragg reflections for SiO_2 (from the mortar and pestle). The asterisk indicates a small amount of boron impurity. Rietveld agreement factors: $\chi^2 = 3.28$; $wR_p = 14.0\%$; $R_p = 14.4\%$; $R(F^2) = 6.08\%$.

Experimental

The starting materials for the synthesis of polycrystalline $WB_{4.2}$ were boron (99.5%, chunk, Johnson Matthey Catalog Co.) and tungsten powder (>99.9%, Alfa). The tungsten powder was pressed into a pellet and arc-melted to have a metal chunk for the subsequent melting. The W and B chunks were weighed out in a 1:10 ratio and arc-melted three times in a Zr-gettered Ar atmosphere of ~600 mbar. The arc-melted buttons were flipped in between each melting to ensure homogeneous samples. The resulting sample buttons had <1% mass loss and are stable in air over time. High quality samples of $WB_{4.2}$ are only obtained when a significant excess of B is employed, as has been previously reported [36]. The purity of all samples was checked at room temperature using a Bruker D8 Advance Eco Cu Kα radiation ($\lambda = 1.5406$ Å) x-ray diffractometer equipped with a LynxEye-XE detector. Single crystals from arc-melted samples were mounted on the tips of Kapton loops and room-temperature intensity data were collected using a Bruker Apex II x-ray diffractometer with Mo Kα_1 radiation ($\lambda = 0.710\,73$ Å). All data were collected with 0.5° scans in ω over a full sphere of reciprocal space with 10 s per frame of exposure time. Data acquisition was carried out using the SMART software. The program VESTA was used to create all crystal structure images [37]. The SAINT program was used to both extract and correct intensities for polarization and Lorentz effects. XPREP, which is based on face-indexed absorption, was used for numerical absorption corrections [38]. The unit cell was tested for twinning. The crystal structure was then solved using direct methods with the SHELXTL package and the refinement was carried out by full-matrix least squares on F^2 [39]. A Rietveld refinement of the room temperature powder x-ray diffraction (pXRD) data was performed using the FullProf Suite program with Thompson–Cox–Hastings pseudo-Voigt peak shapes and the lattice parameters from the single crystal refinement as a starting point.

Table 1. Single crystal crystallographic data for $WB_{4.2(1)}$ at 293 (2) K.

Formula	$WB_{4.2(1)}$
F.W. (g mol^{-1})	229.33
Space group	$P6_3/mmc$ (No.194)
a (Å)	5.191(6)
c (Å)	6.345(8)
V (Å^3)	148.0(4)
Absorption correction	Numerical
Extinction coefficient	0.014(2)
No. reflections; R_{int}	874; 0.0833
No. independent reflections	151
No. parameters	15
R_1; wR_2 ($I > 2\sigma(I)$)	0.0327; 0.0573
R_1; wR_2 (all I)	0.0556; 0.0606
Goodness of fit	1.130
Diffraction peak and hole (e$^-$ Å^{-3})	2.640; –3.284

A superconducting quantum interference device with a ^{3}He attachment was used to measure the zero-field cooled (ZFC) temperature-dependent volume magnetic susceptibility from 0.5 to 2.2 K with $H = 20$ Oe as the applied magnetic field. The field-dependent magnetization was measured at 1.4, 1.0, and 0.5 K from 0 to 35 Oe. A physical property measurement system equipped with a resistivity option and ^{3}He attachment was used to measure the temperature-dependent electrical resistivity from 300 to 0.5 K under zero applied magnetic field using a standard four probe method. The low

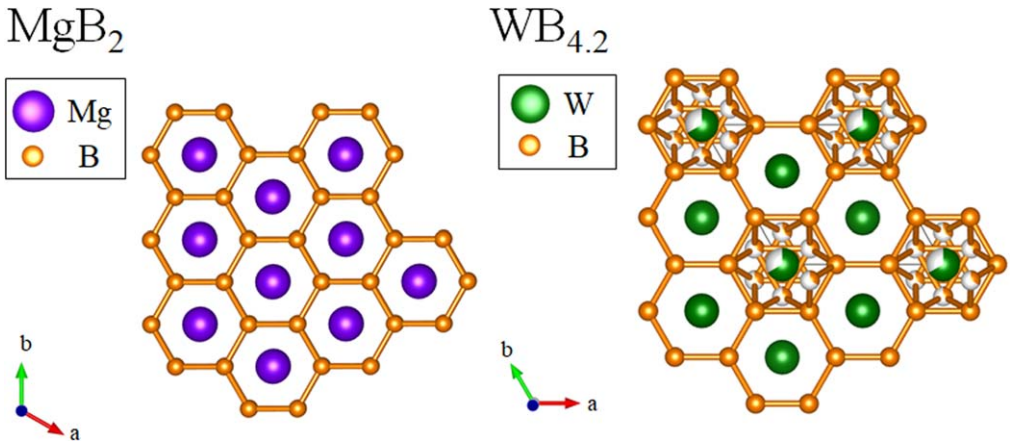

Figure 2. Comparison of the crystal structures of MgB_2 (left) and $WB_{4.2}$ (right). Boron atoms are shown in orange, magnesium atoms in purple, and tungsten in green.

temperature resistivity was measured under applied magnetic fields ranging from 0 to 600 mT in the temperature region from 0.5 to 2.2 K. The specific heat was measured on a small polished sample of polycrystalline $WB_{4.2}$ using Apiezon N grease from 3.6 to 0.5 K under zero applied magnetic field.

Results and discussion

The crystal structure of $WB_{4.2}$ was analyzed using single crystal x-ray diffraction, which showed that the superconductor crystallizes in the space group $P6_3/mmc$ (No. 194) with lattice parameters $a = 5.191(6)$ Å and $c = 6.345(8)$ Å, consistent with what has been previously reported [36]. Figure 1 shows a Rietveld refinement of the room temperature pXRD data for $WB_{4.2}$ using the lattice parameters and the space group from the single crystal refinement as a starting point. It should be noted that there is some SiO_2 in the pXRD pattern (indicated by the light green vertical bars in figure 1) that originates from parts of the agate mortar and pestle that intrude during grinding due to the superhardness of $WB_{4.2}$. The lattice parameters and the W occupancy from both refinements are in good agreement with one another so only the single crystal refinement will be discussed here. The results from the single crystal refinement are shown in table 1 and the atomic coordinates from the same refinement are given in table 2 for $WB_{4.2}$. The W2 atom position was freely refined, resulting in an occupancy of 0.665, and, consistent with the previous report, three B atoms were found in a triangular arrangement in place of the missing W2 atoms [36]. Figure 2 shows a comparison of the crystal structure of $WB_{4.2}$ (right) and MgB_2 (left). The boron atoms in MgB_2 form a honeycomb network, similar to graphite, with the magnesium atoms between the upper and lower six-membered rings that form the hexagonal honeycomb layers. $WB_{4.2}$ has a similar boron honeycomb with some of the holes between layers fully occupied by only W atoms while other holes can be occupied either by W2 or a B_3 triangle. Although the occupancy of 0.665 for the W2 position is within error of a value of 2/3,

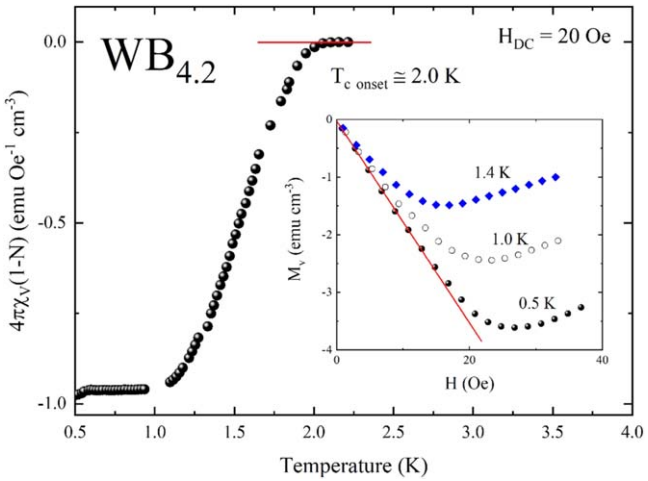

Figure 3. Temperature dependence of ZFC volume magnetic susceptibility (χ_V) measured in a 20 Oe applied magnetic field. Inset: volume magnetization (M_V) versus field at 0.5, 1.0 and 1.4 K.

which has the potential to result in a long range ordered structure, no evidence for W2 ordering is observed, consistent with previous reports [30]. The structure can be considered as either a highly defective or highly non-stoichiometric version of WB_2. There is also no crystallographic evidence for a wide range in stoichiometry for this compound [36].

The temperature-dependent volume magnetic susceptibility (χ_V) was measured to characterize the superconducting critical temperature of $WB_{4.2}$. The ZFC χ_V versus T (figure 3) shows the first clear deviation from the normal state susceptibility at approximately 2.0 K. The volume magnetization (M_V) was measured at 1.4, 1.0, and 0.5 K from 0 to 35 Oe as shown in the inset of figure 3. At low magnetic fields ($H < 15$ Oe) the M_V data collected at 0.5 K was fitted with the linear formula $M_v(H) = -bH$, where b is the slope of the fitted line. Assuming that the initial linear response to an applied magnetic field is perfectly diamagnetic ($dM_v/dH = -1/[4\pi(1-N)]$), we obtained a demagnetization factor $N = 0.55$. The main panel of figure 3 shows the volume magnetic susceptibility in

Table 2. Atomic coordinates and equivalent isotropic displacement parameters of $WB_{4.2(1)}$ at 293(2) K. U_{eq} is defined as one-third of the trace of the orthogonalized U_{ij} tensor (Å^2).

Atom	Wyckoff	Occupancy	x	y	z	U_{eq}
W1	2*c*	1	2/3	1/3	¼	0.0029(3)
W2	2*b*	0.665(8)	0	0	¼	0.0038(4)
B1	12*i*	1	0.335(4)	0	0	0.005(2)
B2	6*h*	0.335[a]	0.115(5)	0.229(9)	¼	0.008(3)

[a] The W2 position occupancy is freely refined, but the fractional occupancy of the B2 site is constrained such that the occupancy of B2 = 1 − occupancy of W2, as described in previous studies [36]. The positional parameters of B2 are freely refined.

the presence of a demagnetization effect ($N = 0.55$) and normalized by 4π. The tiny departure of the strongest diamagnetic signal at the lowest temperatures from -1, which corresponds to perfect diamagnetism, is most likely due to mass error from working with such a small sample. A rough estimation of the lower critical field at 0.5 K (not corrected for demagnetization) is $H_{c1}(0.5\ \mathrm{K}) = 10$ Oe.

The inset of figure 4 shows C_p/T versus T^2, where the data were fitted above the critical temperature to the equation,

$$\frac{C_p}{T} = \gamma + \beta T^2,$$

where γT is the electronic contribution (C_{el}) to the specific heat and βT^3 is the phonon contribution (C_{ph}). The slope of the fitted line, β, is 0.021(1) mJ mol^{-1} K^{-4} and the Sommerfeld parameter, γ, is calculated to be 2.07(3) mJ mol^{-1} K^{-2}. Using β, the Debye temperature (Θ_D) is calculated to be 780(10) K using the equation

$$\Theta_D = \left(\frac{12\pi^4}{5} nR\right)^{\frac{1}{3}},$$

where R is the ideal gas constant 8.314 J mol^{-1} K^{-1} and $n = 5.2$ for $WB_{4.2}$. The Debye temperature is high, which reflects a high concentration of boron (for which $\Theta_D = 1300$ K [40]) in the material. With Θ_D, T_c, and assuming $\mu^* = 0.13$, the inverted McMillan formula [41]

$$\lambda_{ep} = \frac{1.04 + \mu^* \ln\left(\frac{\Theta_D}{1.45T_c}\right)}{(1 - 0.62\mu^*)\ln\left(\frac{\Theta_D}{1.45T_c}\right) - 1.04}$$

can be used to calculate the electron–phonon coupling constant λ_{ep} to be 0.43 for $WB_{4.2}$. The Fermi energy $N(E_F)$ is calculated with the formula

$$N(E_F) = \frac{3\gamma}{\pi^2 k_B^2 (1 + \lambda_{ep})}$$

to be 0.61 states eV^{-1} per formula unit of $WB_{4.2}$ where $\gamma = 2.07(3)$ mJ mol^{-1} K^{-2}, $\lambda_{ep} = 0.43$, and k_B is the Boltzmann constant.

The main panel of figure 4 shows the electronic specific heat divided by temperature (C_{el}/T) versus temperature for $WB_{4.2}$ from 0.5 to 3.6 K with zero applied magnetic field showing a large peak in the specific heat. C_{el} was obtained by subtracting the phonon contribution to the specific heat: $C_{el} = C_p - \beta T^3$. The T_c is estimated to be 2.05 K for this data using an equal-area entropy construction (solid black lines), which is close to the critical temperature from the temperature-dependent magnetic susceptibility measurement. Such a large peak in the specific heat due to a significant loss of entropy is an explicit indication that the bulk material is superconducting. The normalized specific heat jump, $\Delta C/\gamma T_c$, is estimated as 1.56 for $WB_{4.2}$, which is near the weak coupling BCS limit of 1.43 [42] and confirms that $WB_{4.2}$ is a bulk superconductor.

Figure 5 shows $C_{el} - \gamma_0 T$ versus T_c/T for $WB_{4.2}$ in the superconducting state under zero applied magnetic field and fitted to the following equation

$$C_{el.} = \gamma_0 T + a^* e^{-\frac{\Delta_0}{k_B T}},$$

where $\gamma_0 T$ is the electronic contribution to the specific heat originating from impurities in the sample, Δ_0 is the superconducting gap magnitude, and k_B is the Boltzmann constant. The Δ_0 for $WB_{4.2}$ was calculated to be $\Delta_0 = 0.22$ meV and according to BCS theory [42], it is expected to be

$$2\Delta_0 = 3.5\ k_B T_c$$

for a weak coupling superconductor. The calculated value of the superconducting gap $\Delta_0 = 0.22$ meV ($2\Delta_0 = 0.44$ meV) is less than the weak coupling BCS value of $2\Delta_0 = 0.62$ meV. The discrepancy may indicate that multiband superconductivity may be present in this material.

Figure 6 shows the temperature-dependent electrical resistivity for $WB_{4.2}$ measured from 300 to 1.7 K. In the normal state, the resistivity changes slightly and the RRR ratio ($\rho_{300K}/\rho_{2.2K}$) is only ~1.3, as is often observed for polycrystalline samples. The inset of figure 6 shows that the resistivity drops to 50% of the normal state value at ~2.1 K (black dotted line) and reaches zero above 2 K. The resistivity transition is sharp and only covers a 0.2 K temperature range. The T_c values from the resistivity, specific heat, and magnetic susceptibility are in agreement.

The inset of figure 7 shows the dependence of the T_c (black line) on the applied magnetic field for $WB_{4.2}$ in the

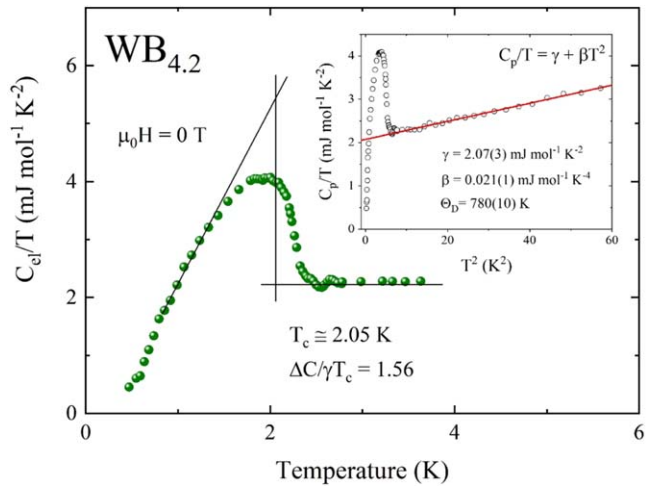

Figure 4. Electronic heat capacity divided by temperature (C_{el}/T) versus temperature measured from 3.6 to 0.5 K under zero applied magnetic field. Inset: C_p/T versus T^2 shown for the low temperature region and fitted to a line.

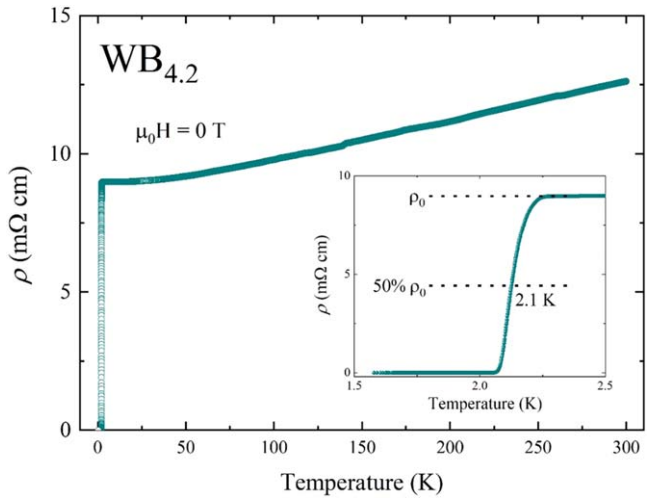

Figure 6. Temperature-dependent resistivity of polycrystalline $WB_{4.2}$ measured from 300 to 1.7 K under zero applied magnetic field. Inset: resistivity near the superconducting transition.

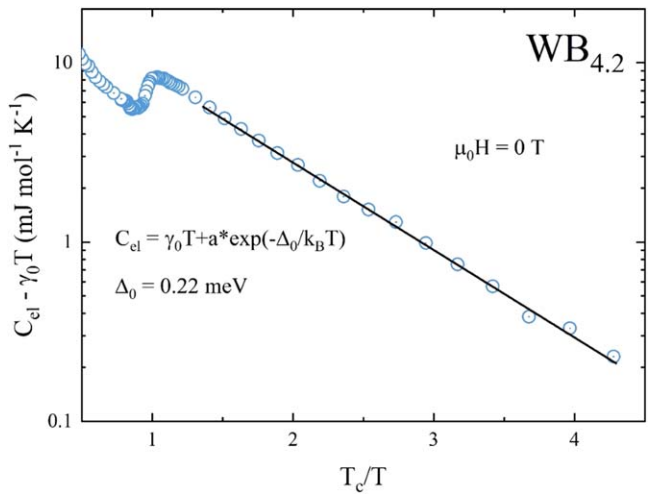

Figure 5. Electronic heat capacity $C_{el.} - \gamma_0 T$ versus the normalized T_c/T for $WB_{4.2}$ to determine the superconducting gap Δ_0.

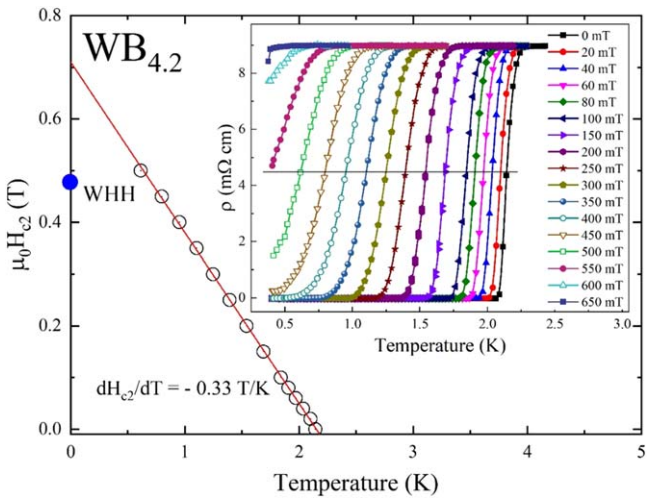

Figure 7. Upper critical field ($\mu_0 H_{c2}$) versus temperature fitted to a line. Inset: ρ versus T under various magnetic fields showing the dependence of the T_c on the applied field. The solid black line shows 50% of the superconducting transition.

temperature range from 0.5 to 2.2 K under applied magnetic fields ranging from 0 to 600 mT. The T_c steadily decreases with increasing applied field, as expected, and the last instance where the resistivity drops to below 50% is for $T_c = 0.62$ K with $\mu_0 H = 500$ mT. The thus-determined upper critical fields ($\mu_0 H_{c2}$) plotted as a function of the estimated T_c values were plotted in the main panel of figure 7 and fitted to a line with slope $d\mu_0 H_{c2}/dT = -0.33\,\mathrm{T\,K^{-1}}$. For many superconductors, the zero temperature upper critical field $\mu_0 H_{c2}(0)$ can be estimated with the Werthamer–Helfand–Hohenberg (WHH) [43] equation given by:

$$\mu_0 H_{c2}(0) = -AT_c \frac{d\mu_0 H_{c2}}{dT}\bigg|_{T=T_c},$$

where A is -0.693 for the dirty limit and taking T_c as $\sim$2.05 K for $WB_{4.2}$. Based on this model, the $\mu_0 H_{c2}(0) = 0.47$ T (indicated by the blue closed circle in figure 7), however the last measured $\mu_0 H_{c2}$ value is 0.50 T which is already above the WHH-predicted upper critical field of 0.47 T. The nearly linear $H_{c2}(T)$ over a broad temperature range that we observe has been seen previously for Fe based superconductors [44, 45] and also for $Nb_2Pd_{0.81}S_5$[46] and claimed to originate from the multiband superconductivity effect. The resulting $\mu_0 H_{c2}(0)$ for $WB_{4.2}$ is therefore most likely somewhere between the linear extrapolation to 0 K (0.71 T) and that predicted by the WHH model (0.47 T). Taking $\mu_0 H_{c2}(0) = 0.71$ T as the upper limit, the approximate coherence length can be calculated by using the Ginzburg–Landau formula $\xi_{GL}(0) = \{\phi_0/[2\pi H_{c2}(0)]\}^{1/2}$, where $\phi_0 = h/2e$ and is found to be $\xi_{GL}(0) = 26$ nm. All physical parameters for $WB_{4.2}$ are gathered in table 3.

Table 3. Normal and superconducting state parameters for $WB_{4.2}$.

Parameter	Unit	Value
T_c	K	2.05(5)
$\mu_0 H_{c2}(0)$	T	0.71
λ_{ep}	—	0.43
$\xi_{GL}(0)$	nm	26
γ	mJ mol^{-1} K^{-2}	2.07(3)
β	mJ mol^{-1} K^{-4}	0.021(1)
Θ_D	K	780(10)
$\Delta C/\gamma T_c$	—	1.56
Δ_0	meV	0.22
DOS(E_F)	states eV^{-1} f.u.$^{-1}$	0.61

Conclusions

We report superconductivity in the superhard material $WB_{4.2}$ and confirm that this material crystallizes in the hexagonal space group $P6_3/mmc$ using room-temperature single crystal x-ray diffraction data. This material is non-stoichiometric via W deficiency, where for every missing W atom, three B atoms are inserted into the structural cavity in its place. The superconducting transition occurs at about 2 K and is characterized through temperature-dependent magnetic susceptibility, electrical resistivity, and specific heat measurements. $WB_{4.2}$ is shown to be a BCS-type weak coupled superconductor based on the calculated superconducting parameters. The $\mu_0 H_{c2}(0)$ value is between the value predicted using the WHH model and that of a linear extrapolation of $\mu_0 H_{c2}(T)$ to 0 K. This material appears to be an example of a highly non-stoichiometric, metal deficient, early transition metal diboride superconductor.

Acknowledgments

The materials synthesis was supported by the Department of Energy, Division of Basic Energy Sciences, Grant DE-FG02-98ER45706, and the property characterization at Princeton was supported by the Gordon and Betty Moore Foundation EPiQS initiative, Grant GBMF-4412. The research at the Gdansk University of Technology was supported by the National Science Centre, Grant UMO−2016/22/M/ST5/00435. The work in the Department of Chemistry at LSU was supported by the US Department of Energy under EPSCoR Grant No. DE-SC0012432 with additional support from the Louisiana Board of Regents. The authors declare that they have no competing interests.

ORCID iDs

Elizabeth M Carnicom https://orcid.org/0000-0001-7895-5147
P Wiśniewski https://orcid.org/0000-0002-6741-2793
T Klimczuk https://orcid.org/0000-0002-7089-4631

References

[1] Nagamatsu J, Nakagawa N, Muranaka T, Zenitani Y and Akimitsu J 2001 Superconductivity at 39 K in magnesium diboride *Nature* **410** 63–4
[2] Muzzy L E, Avdeev M, Lawes G, Haas M K, Zandbergen H W, Ramirez A P, Jorgensen J D and Cava R J 2002 Structure and superconductivity in Zr-stabilized, nonstoichiometric molybdenum diboride *Physica* C **382** 153–65
[3] Akimitsu J 2001 *Annual Meeting Phys. Soc. Japan* p 533
[4] Carnicom E M, Xie W, Klimczuk T, Lin J, Górnicka K, Sobczak Z, Ong N P and Cava R J 2018 $TaRh_2B_2$ and $NbRh_2B_2$: superconductors with a chiral noncentrosymmetric crystal structure *Sci. Adv.* **4** eaar7969
[5] Kayhan M, Hildebrandt E, Frotscher M, Senyshyn A, Hofmann K, Alff L and Albert B 2012 Neutron diffraction and observation of superconductivity for tungsten borides, WB and W_2B_4 *Solid State Sci.* **14** 1656–9
[6] Xie W W, Luo H, Baroudi K, Krizan J W, Phelan B F and Cava R J 2015 Fragment-based design of NbRuB as a new metal-rich boride superconductor *Chem. Mater.* **27** 1149–52
[7] Zheng Q, Gumeniuk R, Rosner H, Schnelle W, Prots Y, Burkhardt U, Grin Y and Leithe-Jasper A 2015 Synthesis, crystal structure and properties of the new superconductors TaRuB and NbOsB *J. Phys.: Condens. Matter* **27** 415701
[8] Escamilla R, Lovera O, Akachi T, Durán A, Falconi R, Morales F and Escudero R 2004 Crystalline structure and the superconducting properties of NbB_{2+x} *J. Phys.: Condens. Matter* **16** 5979–90
[9] Yamamoto A, Takao C, Masui T, Izumi M and Tajima S 2002 High-pressure synthesis of superconducting $Nb_{1-x}B2$ ($x = 0$–0.48) with the maximum $T_c = 9.2$ K *Physica* C **383** 197–206
[10] Nunes C A, Kaczorowski D, Rogl P, Baldissera M R, Suzuki P A, Coelho G C, Grytsiv A, André G, Boureé F and Okada S 2005 The NbB_2-phase revisited:homogeneity range, defect structure, superconductivity *Acta Mater.* **53** 3679–87
[11] Kaner R B, Gilman J J and Tolbert S H 2005 Designing superhard materials *Science* **308** 1268–70
[12] Yin S *et al* 2013 Hardness and elastic moduli of high pressure synthesized MoB_2 and WB_2 compacts *High Press. Res.* **33** 409–17
[13] Xie M, Mohammadi R, Mao Z, Armentrout M M, Kavner A, Kaner R B and Tolbert S H 2012 Exploring the high-pressure behavior of superhard tungsten tetraboride *Phys. Rev.* B **85** 064118
[14] Qin J, He D, Wang J, Fang L, Lei L, Li Y, Hu J, Kou Z and Bi Y 2008 Is rhenium diboride a superhard material? *Adv. Mater.* **20** 4780–3
[15] Zhang R F, Lin Z J, Zhao Y S and Veprek S 2011 Superhard materials with low elastic moduli: three-dimensional covalent bonding as the origin of superhardness in B_6O *Phys. Rev.* B **83** 092101
[16] Gu Q, Krauss G and Steurer W 2008 Transition metal borides: superhard versus ultra-incompressible *Adv. Mater.* **20** 3620–6
[17] Wang M, Li Y, Cui T, Ma Y and Zou G 2008 Origin of hardness in WB_4 and its implications for ReB_4, TaB_4, MoB_4, TcB_4, and OsB_4 *Appl. Phys. Lett.* **93** 101905
[18] Levine J B, Tolbert S H and Kaner R B 2009 Advancements in the search for superhard ultra-incompressible metal borides *Adv. Funct. Mater.* **19** 3519–33
[19] Sung C M and Sung M 1996 Carbon nitride and other speculative superhard materials *Mater. Chem. Phys.* **43** 1–18
[20] Thornton A G and Wilks J 1978 Clean surface reactions between diamond and steel *Nature* **274** 792–3

[21] Komanduri R and Shaw M C 1975 Wear of synthetic diamond when grinding ferrous metals *Nature* **255** 211–3
[22] Taniguchi T, Akaishi M and Yamaoka S 1996 Mechanical properties of polycrystalline translucent cubic boron nitride as characterized by the Vickers indentation method *J. Am. Ceram. Soc.* **79** 547–9
[23] Solozhenko V L, Andrault D, Fiquet G, Mezouar M and Rubie D C 2001 Synthesis of superhard cubic BC_2N *Appl. Phys. Lett.* **78** 1385–7
[24] Cumberland R W, Weinberger M B, Gilman J J, Clark S M, Tolbert S H and Kaner R B 2005 Osmium diboride, an ultra-incompressible, hard material *J. Am. Chem. Soc.* **127** 7264–5
[25] Chung H Y, Weinberger M B, Yang J M, Tolbert S H and Kaner R B 2008 Correlation between hardness and elastic moduli of the ultraincompressible transition metal diborides RuB_2, OsB_2, and ReB_2 *Appl. Phys. Lett.* **92** 261904
[26] Chung H Y, Yang J-M, Tolbert S H and Kaner R B 2008 Anisotropic mechanical properties of ultra-incompressible, hard osmium diboride *J. Mater. Res.* **23** 1797–801
[27] Simunek A 2009 Anisotropy of hardness from first principles: the cases of ReB_2 and OsB_2 *Phys. Rev.* B **80** 060103
[28] Chung H, Weinberger M B, Levine J B, Kavner A, Yang J M, Tolbert S H and Kaner R B 2007 Synthesis of ultra-incompressible superhard rhenium diboride at ambient pressure *Science* **316** 436–9
[29] Gou H *et al* 2013 Discovery of a superhard iron tetraboride superconductor *Phys. Rev. Lett.* **111** 157002
[30] Jiang C, Pei Z, Liu Y, Xiao J, Gong J and Sun C 2013 Preparation and characterization of superhard AlB_2-type WB_2 nanocomposite coatings *Phys. Status Solidi* A **210** 1221–7
[31] Itoh H, Matsudaira T, Naka S, Hamamoto H and Obayashi M 1987 Formation process of tungsten borides by solid state reaction between tungsten and amorphous boron *J. Mater. Sci.* **22** 2811–5
[32] Romans P A and Krug M P 1966 Composition and crystallographic data for the highest boride of tungsten *Acta Cryst.* **20** 313–5
[33] Chretien A and Helgorsky J 1961 Borides of molybdenum and tungsten, MoB_4 and WB_4; new compounds *Compt. Rend.* **252** 742–4
[34] Nowotny H, Haschke H and Benesovsky F 1967 Bor-reiche wolframboride *Monatsh. Chem.* **98** 547–54
[35] Zeiringer I, Rogl P, Grytsiv A, Polt J, Bauer E and Giester G 2014 Crystal structure of $W_{1-x}B_3$ and phase equilibria in the boron-rich part of the systems Mo–Rh–B and W-{Ru,Os,Rh, Ir,Ni,Pd,Pt}-B *J. Phase Equilibria Diffus.* **35** 384–95
[36] Lech A T, Turner C L, Mohammadi R, Tolbert S H and Kaner R B 2015 Structure of superhard tungsten tetraboride: a missing link between MB_2 and MB_{12} higher borides *Proc. Natl Acad. Sci.* **112** 3223–8
[37] Momma K and Izumi F 2011 VESTA 3 for three-dimensional visualization of crystal, volumetric and morphology data *J. Appl. Crystallogr.* **44** 1272–6
[38] 2000 SHELXTL Software Reference Manual, Version 6.10, Bruker Analytical X-Ray System, Inc. (Madison, WI)
[39] Sheldrick G M 2008 A short history of SHELX *Acta. Crystallogr.* A **64** 112–22
[40] Slack G A 1965 Thermal conductivity of elements with complex lattices: B, P, S *Phys. Rev.* **139** A507–15
[41] McMillan W L 1968 Transition temperature of strong-coupled superconductors *Phys. Rev.* **167** 331–44
[42] Tinkham M 1996 *Introduction to Superconductivity* (Mineola, NY: Dover)
[43] Werthamer N R, Helfand E and Hohenberg P C 1966 Temperature and purity dependence of the superconducting critical field, H_{c2}: III. Electron spin and spin-orbit effects *Phys. Rev.* **147** 295–302
[44] Yamamoto A *et al* 2009 Small anisotropy, weak thermal fluctuations, and high field superconductivity in Co-doped iron pnictide $Ba(Fe_{1-x}Co_x)_2As_2$ *Appl. Phys. Lett.* **94** 062511
[45] Yuan H Q, Singleton J, Balakirev F F, Baily S A, Chen G F, Luo J L and Wang N L 2009 Nearly isotropic superconductivity in (Ba, K)Fe_2As_2 *Nature* **457** 565–8
[46] Zhang Q, Li G, Rhodes D, Kiswandhi A, Besara T, Zeng B, Sun J, Siegrist T, Johannes M D and Balicas L 2013 Superconductivity with extremely large upper critical fields in $Nb_2Pd_{0.81}S_5$ *Sci. Rep.* **3** 1446